ELSEVIER

Chemical Engineering Journal 138 (2008) 474–489

Chemical Engineering Journal

www.elsevier.com/locate/cej

A micro-structured 5 kW complete fuel processor for iso-octane as hydrogen supply system for mobile auxiliary power units Part II—Development of water–gas shift and preferential oxidation catalysts reactors and assembly of the fuel processor

Gunther Kolb [a,*], Tobias Baier [a], Jochen Schürer [a], David Tiemann [a], Athanassios Ziogas [a], Stefania Specchia [b], Camilla Galletti [b], Gabriele Germani [c], Yves Schuurman [c]

[a] *Institut für Mikrotechnik Mainz (IMM), Germany*

[b] *Dipartimento di Scienza dei Materiali e Ingegneria Chimica – Politecnico di Torino, Torino, Italy*

[c] *Institut de Recherches sur la Catalyse, CNRS, 2 Avenue Albert Einstein, 69626 Villeurbanne, France*

Received 8 January 2007; received in revised form 27 June 2007; accepted 30 June 2007

Abstract

Microstructured reactors for water–gas shift and the preferential oxidation of carbon monoxide were developed for a fuel processing/fuel cell system running on iso-octane and designed for an electrical power output of 5 kW_{el}. The target application was an automotive auxiliary power unit (APU). The work covered both catalyst and reactor development. A platinum/ceria catalyst was applied for water–gas shift, while platinum on zeolite/alumina carrier served as catalyst for preferential oxidation. These catalysts were introduced into the final full size prototype reactors, which were constructed from microstructured stainless steel foils. Testing in a pilot scale test rig revealed conversion close to the thermodynamic equilibrium for the water–gas shift reactors at a WHSV range of 17–41 $Ndm^3/(h\,g_{cat})$. The preferential oxidation, which was performed at higher WHSV in the range of 48–98 $Ndm^3/(h\,g_{cat})$ revealed up to 90% conversion in a first stage, while in the second stage reactor the carbon monoxide content of the reformate was decreased to less than 50 ppm. The reactors were then incorporated into a complete bread-board fuel processor of 5 kW_{el} power equivalent, which comprised also of an autothermal reformer reactor. The fuel processor was operated at a steam to carbon ratio of 3.3 and an oxygen to carbon ratio of 0.67. Under these conditions, it converted the iso-octane feed completely to purified reformate with an overall efficiency of 74%.

Keywords: Microchannels; Micro-reactor; Water–gas shift; Preferential oxidation; Fuel processor

1. Introduction

Hydrogen supply for fuel cell systems is a critical issue in case of mobile applications. One viable option is fuel processing of liquid fuels, which is most attractive for automotive applications owing to the existing fuel storage capacity. The current paper deals with the development of a complete microstructured fuel processor for a 5 kW_{el} automotive fuel cell auxillary power unit (APU) running on iso-octane. In a former paper, the development of the autothermal reformer catalyst and reactor had been described, the current paper covers the catalytic carbon monoxide clean-up units and the assembly and testing of the complete fuel processor.

The reformate formed during reforming of all kind of carbonaceous fuels contains beside the desired hydrogen also carbon dioxide, steam, nitrogen (not for steam reforming) and carbon monoxide. In case of hydrocarbon fuel processing, the carbon monoxide content of the reformate ranges between 5 and 15 vol.% depending on the reforming strategy chosen.

Proton exchange membrane (PEM) fuel cells are regarded as most promising candidates for small scale mobile and portable APU systems in the power range exceeding several hundreds of Watts. In case high temperature PEM fuel cells are applied, the content of carbon monoxide in the reformate needs to be reduced to values around 1 vol.%. Low temperature PEM fuel cells are even more sensible to poisoning by carbon monoxide

* Corresponding author.
E-mail address: Kolb@imm-mainz.de (G. Kolb).

1385-8947/$ – see front matter © 2007 Elsevier B.V. All rights reserved.
doi:10.1016/j.cej.2007.06.037

and require a carbon monoxide content between 10 ppm and several hundred ppm depending on the membrane technology applied.

The carbon monoxide clean-up for small scale applications is usually done by catalytic purification reactions, because alternative technologies such as pressure or temperature swing adsorption add too much space to the power generation system. Membrane separation offers an alternative despite the elevated pressure required for certain applications. In the current paper, low temperature PEM fuel cell technology was chosen and the catalytic clean-up strategy was applied thus comprising of both water–gas shift (WGS) and preferential oxidation (PrOx) of carbon monoxide.

Microstructured plate heat exchanger reactor technology was applied, which bears a number of advantages compared to conventional technology such as fixed catalyst beds, namely lower pressure drop and enhanced heat and mass transfer [1]. When plate heat exchangers are coated with catalyst, the heat generated by exothermic reactions may be removed improving the thermal management of the reactor [2]. Delsman et al. demonstrated the feasibility of integrated cooling for preferential oxidation in the power range of 100 W in a microstructured heat-exchanger/reactor [3].

The current paper provides in Section 2 an overview of the reaction systems of water–gas shift and preferential oxidation of carbon monoxide. Then reactor development is described in Section 3, which covers both a specially designed testing reactor and the final prototype reactors. In Section 4, catalyst development is summarised, which was performed both for water–gas shift and preferential oxidation of carbon monoxide. The four final carbon monoxide clean-up reactors designed for a 5 kW auxiliary power unit were then tested separately in a dedicated test rig. Results from these tests are summarised in Section 5. Finally, three of these reactors along with a heat-exchanger and an autothermal reformer reactor, the development of which was reported in a previous paper [4], were incorporated into a bread board fuel processor an operated together, which is subject of Section 6 of the current paper.

2. Reaction system and feed composition

2.1. Water–gas shift

Autothermal reforming was chosen for the system described here. Applying air as oxygen source relates to the following basic formula for iso-octane assuming a steam to carbon ratio (S/C) of 2.7 and about 22 vol.% water remaining in the fuel cell feed [4]:

$$3\,C_8H_{18} + 8\,O_2 + 32\,N_2 + 64\,H_2O \rightarrow 32\,H_2 + 24\,CO + 32\,N_2 + 56\,H_2O \quad \Delta H_{298} \approx 0\,\text{kJ/mol}$$

However, water–gas shift takes already place in the reformer reactor. Additionally a higher S/C was applied in the current system and thus the feed composition of the WGS reactor is slightly different which will be discussed below.

The water–gas shift reaction itself:

$$CO + H_2O \rightarrow CO_2 + H_2 \qquad \Delta H_{298} = -41\,\text{kJ/mol}$$

is limited by its thermodynamic equilibrium, which may be calculated according to the formula provided below [5]:

$$K_{eq} = \exp\left(\frac{4577.8}{T} - 4.33\right) \tag{2}$$

Because subsequent carbon monoxide-clean-up by carbon monoxide PrOx follow the shift reactor downstream as mentioned above, the carbon monoxide content of water–gas shift reactor off-gas should not exceed 1 vol.%. A trade-off is required between carbon monoxide-level and reactor size owing to the lower reaction temperatures required from the thermodynamic equilibrium. To limit the reactor size, water–gas shift is usually performed in two stages with intermediate cooling preferably by water injection [6]. In the first stage, the so-called high-temperature water–gas shift (HTS), most of the carbon monoxide is converted at high reaction rate. This is performed industrially at temperatures between 350 and 450 °C over Fe_2O_3/Cr_2O_3. These catalysts are robust but suffer from low activity, which is less crucial for the industrial process rather than for a compact fuel processor application. The second stage (low-temperature water–gas shift, LTS) works in the temperature range between 200 and 300 °C over CuO/ZnO catalysts based upon alumina carrier. These catalysts are known to be sensitive to poisoning [7] and short-term temperature peaks. On top of that they are pyrophoric and thus sensitive to air exposure, which is unfavourable for fuel processor operation, especially during start-up procedures.

A side reaction, which may take place in parallel under the conditions of water–gas shift specially over PGM metals is the methanation reaction, which consumes valuable hydrogen:

$$CO + 3H_2 \rightarrow CH_4 + H_2O \qquad \Delta H_R = -215\,\text{kJ/mol}$$

2.2. Preferential oxidation of carbon monoxide

The removal of the remaining carbon monoxide from the product of water–gas shift is commonly performed by the oxidation with air [8]:

$$CO + 0.5\,O_2 \rightarrow CO_2 \qquad \Delta H_R = -283\,\text{kJ/mol}$$

The reaction is accompanied by the undesired side reaction of part of the hydrogen present in the reaction mixture:

$$H_2 + 0.5\,O_2 \rightarrow H_2O \qquad \Delta H_R = -242\,\text{kJ/mol}$$

Another problem occurring in PrOx reactors is the reproduction of carbon monoxide over the catalyst by the reverse water–gas shift reaction (RWGS) in an oxygen deficient atmosphere.

$$H_2 + CO_2 \rightarrow H_2O + CO \qquad \Delta H_R = +41\,\text{kJ/mol}$$

The thermal management of the reaction system is an extremely critical issue, because the catalysts tend to have nar-

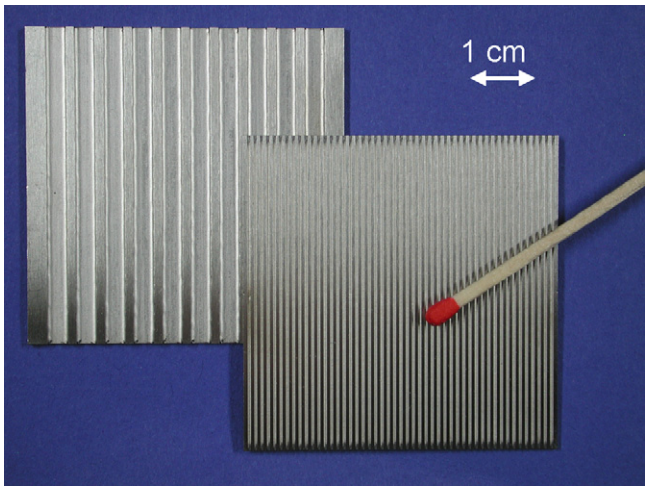

Fig. 1. Different microchannel geometries as realised for the gas-purification testing reactors.

row operating temperature windows. Thus an efficient removal of the heat of the oxidation reactions is required.

3. Reactor development

3.1. Microstructured testing reactor

A testing reactor was designed for the development of the catalyst coatings. It took up either four or six microstructured platelets of different thickness (see Fig. 1). The thicker plates carried 20 channels each 3150 μm wide and 600 μm deep. The thinner platelets had 49 channels each 600 μm wide and 400 μm deep. Both platelets had a length of 50 mm. Because catalyst screening was the target application of the reactor, the platelets needed to be exchangeable. The reactor, an explosion view is shown in Fig. 2, was composed of a housing taking up the platelet stack, which was heated by 6 electrical heating cartridges. The reactor was sealed by graphite gaskets, which limited its operating temperature to 600 °C on the long term. The temperature of the feed and product gas was determined by thermocouples introduced via tubes sealed at one end by welding. They were positioned at the inlet and outlet of the stack of plates (see Fig. 3). An equal flow distribution in the stack of plates was achieved by an inlet diffuser, (see Fig. 3), which was designed for a flow rate of 480 Ncm^3/min similar to a previous design [9]. A pressure drop of 1.7 mbar was calculated for the narrow channel system under these conditions. The maximum operating pressure of the reactor amounted to 8 bar.

3.2. Development of the final 5 kW CO clean-up reactors

The key data of the high-temperature water–gas shift (HTS) and of the other carbon monoxide clean-up reactors discussed below are provided in Table 1. An equal flow distribution was achieved inside the inlet diffusers of each reactor by perforated plates as described in a previous paper [4]. The geometry of the channels was such, that each channel was formed by two half-channels attached face to face. These half-channels had the same dimensions as the channels of the testing reactor. Because the same coating technology and coating thickness was approached for the final reactors and the same weight hourly space velocity had been chosen as identified to be optimum for both water–gas shift and preferential oxidation, equivalent performance was

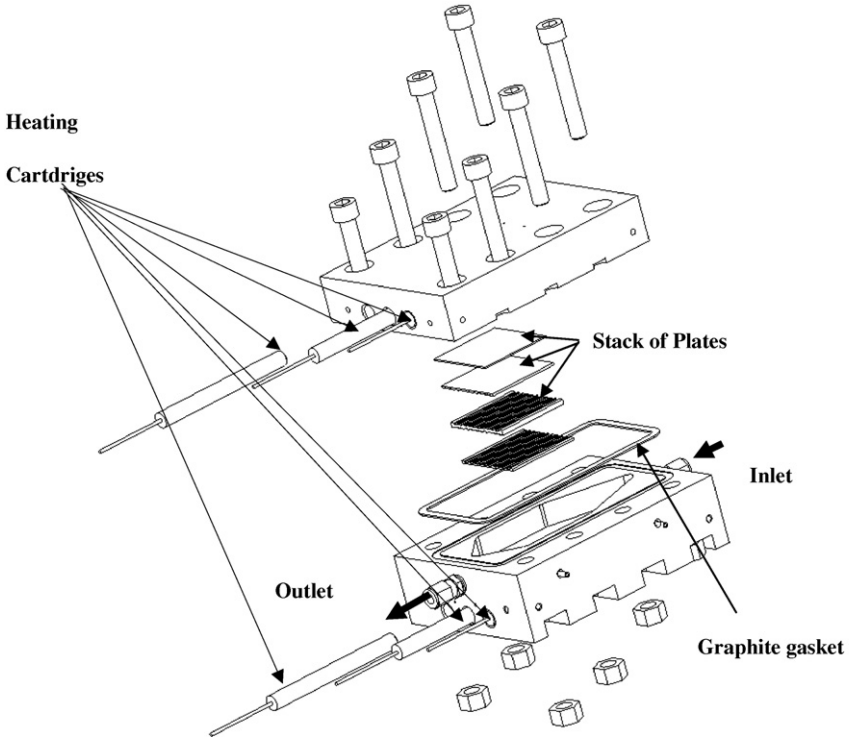

Fig. 2. Explosion view of the gas-purification test reactor.

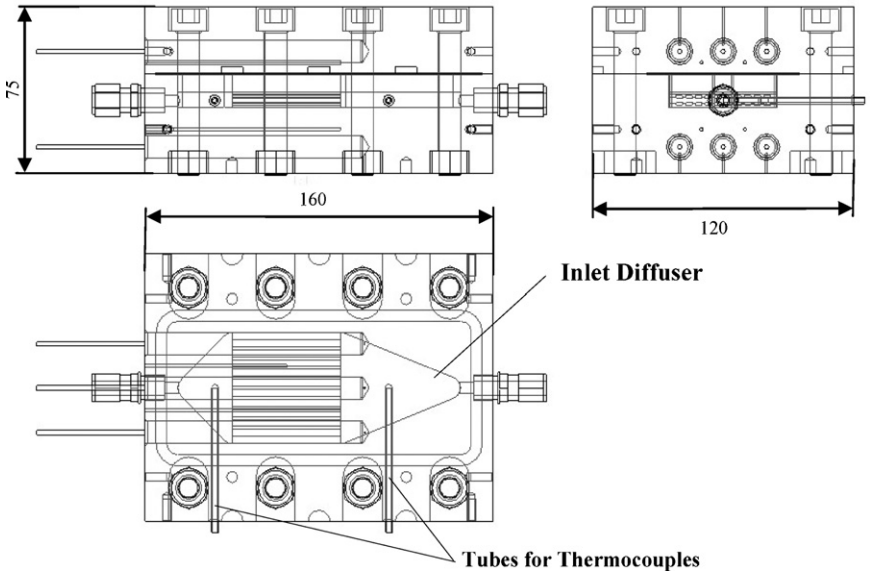

Fig. 3. Technical drawing of the gas-purification test reactor.

to be expected for the final reactors compared to the testing devices.

The HTS carried cross-flow cooling channels, which could be fed by cooling gas in three stages to remove the heat generated by the water–gas shift reaction. Cross-flow cooling had been chosen, because the reactor design and construction is simpler compared to counter-flow. Three cooling stages were introduced to have some flexibility in cooling the inlet, centre and outlet sections of the reactor separately with different flow-rates. Temperature measurement was possible by tubes welded into the reactor body at the inlet and outlet of the reformate and at the outlet of the cooling gas. Additionally, three temperatures could be measured over the length of the reactor axis in a distance of 66 mm, 130 mm and 200 mm downstream the inlet.

The same catalyst as for the HTS was applied for the low temperature water–gas shift reactor (LTS). However, the latter reactor was not designed as a heat-exchanger because of the low heat-generation by low-temperature water–gas shift (calculated to approximately 45 W). This heat was expected to be lost by free convection over the surface of the reactor insulation. Three temperatures could be measured over the length of the reactor axis in a distance of 64 mm, 132 mm and 196 mm downstream the inlet. The reactor was thus composed of a stack of plates, but the functionality was that of a monolithic reactor design.

The WGS reactors were pre-heated electrically to 120 °C by heating cartridges which were incorporated into two plates on top and at the bottom of the reactor. However, most of the pre-

Table 1
Key data of the CO-clean-up reactors

Reactor	HT-WGS cooled (3 stage cross-flow)	LT-WGS un-cooled (monolithic)	1st stage PrOx cooled (3 stage cross-flow)	2nd stage PrOx un-cooled (monolithic)
Max. operating pressure (bar)	4	4	4	4
Max. operating temperature (°C)	450	450	300	300
Reactor dimensions ($L \times W \times H$) (mm)	200 × 120 × 120	200 × 120 × 130	200 × 120 × 120	200 × 120 × 110
Number of foils	110	130	110	110
Foil thickness (mm)	1	1	1	1
Channel dimensions (cooling side) L (mm); $W \times H$ (μm)	120; 2000 × 600	–	120; 2000 × 600	–
Total number of channels	114	0	114	0
Channel dimensions (reactor side) ($W \times H$) (μm)	600 × 800	600 × 800	600 × 800	600 × 800
Channel density (channels/in^2)	720	720	720	720
Total number of channels	13,800	16,380	16,000	16,000
Coated channel surface (m^2)	1.5	1.8	1.5	1.5
Catalyst	1 wt.% Pt/CeO_2 on Al_2O_3	1 wt.% Pt/CeO_2 on Al_2O_3	2 wt.% Pt on zeolite 3A + Al_2O_3	2 wt.% Pt on zeolite 3A + Al_2O_3
Total catalyst mass (g)	232	274	126.5	126.5
WHSV Ndm^3/(h g_{cat})	39–41	17–32	48–87	98

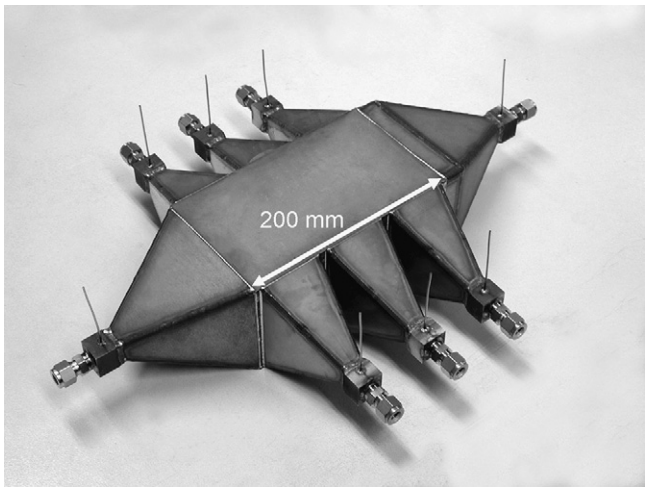

Fig. 4. Final CO-PrOx reactor with three stages cross-flow cooling.

heating up to operating temperature was performed by hot air and steam respectively during start-up.

The heat generation of the carbon monoxide PrOx reaction and of the related hydrogen oxidation is much higher compared to the LTS. Up to 150 K temperature rise was determined for a monolithic PrOx reactor by Ahluwalia et al. [10] at 1.2 vol.% of carbon monoxide in the feed and $\lambda(O/CO) = 2$. Thus cross-flow cooling capabilities were introduced into the corresponding 1st stage carbon monoxide PrOx reactor (PrOx1). Pre-heating of the carbon monoxide PrOx reactors was performed without electrical power, merely with hot start-up gases. Temperature measurement was possible by tubes (see Fig. 4) welded into the reactor body at the inlet and outlet of the reformate and at the outlet of the cooling gas. Additionally, four temperatures could be measured over the length of the reactor axis in a distance of 64 mm, 132 mm and 196 mm downstream the inlet.

Finally, a second stage carbon monoxide-PrOx reactor (PrOx2) was built, which had exactly the same dimensions as the first stage reactor, but did, similar to the LTS reactor, carry no cooling channels and no corresponding inlet and outlet diffusers, because the heat release was expected to be negligible in the second stage preferential oxidation.

4. Catalysts development

4.1. Water–gas shift

Platinum, frequently based upon ceria carrier [11–13] attracted growing attention as alternative to the industrially established water–gas shift catalysts. It may operate in a wide temperature range thus covering both HTS and LTS as medium temperature shift catalyst.

4.1.1. Preparation

An aqueous suspension of alumina powder (Alfa Aesar, 3 mm powder) with a commercial type of methylhydroxyethylcellulose binder (Clariant) was prepared. This suspension was used to slurry-coat the thin platelets (49 channels/plate). The platelets were calcined at 600 °C after coating. The deposited wash-coat inside the microchannels was impregnated to incipient wetness with a cerium precursor solution (4.8 wt.% Ce^{3+} from $Ce(NO_3)_3 \times 6H_2O$, Alfa Aesar: Reaction® 99.5%), using a paintbrush. It was followed by drying and calcination at 400 °C for 2 h. The washcoat was then impregnated six times to incipient wetness with a platinum precursor solution (1.2 wt.% Pt^{2+} from $Pt(NH_3)_4OH_2$, Alfa Aesar: solution, Pt 8–11% w/w), using a paintbrush. The final catalyst coating was calcined for 10 h at 550 °C. The amount of catalyst deposited on each platelet was 106 ± 4 mg.

4.1.2. Catalyst characterisation

A scanning electron microscopy was used to examine the homogeneity and thickness of the wash-coat. A wash-coat in the form of a U-shaped has been observed with only minor cracks. From the micrograph (see Fig. 5) a maximum wash-coat thickness of 39 μm and a minimum thickness of 24 μm has been estimated.

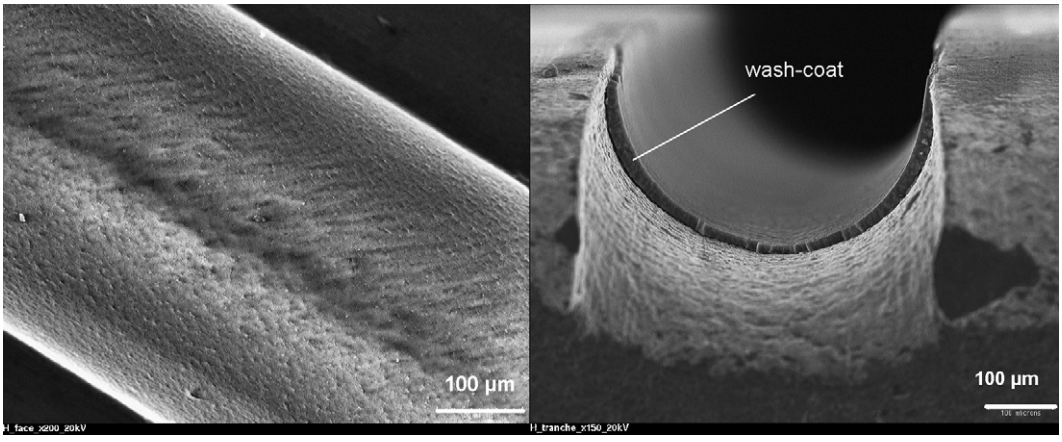

Fig. 5. Scanning transmission micrographs of the $Pt/CeO_2/Al_2O_3$ washcoat deposited inside the microchannels. (a) Channel top view, (b) washcoat layer cross section.

Some of the wash-coat was scraped off the platelets and used for atomic emission spectroscopy analysis. The measured metal weight percentages are as follows:

0.8 wt% of Pt, 3.4 wt% of Ce, 46.4 wt% of Al.

The specific surface area of the scraped-off catalyst was measured by nitrogen adsorption, and compared with the surface of the pure alumina calcined 10 h at 600 °C. The BET surface area of the pure γ-Al_2O_3 was equal to 82 m^2/g, which decreased to 72 m^2/g after impregnation with ceria and the platinum solution.

A platinum dispersion of 67% was measured by hydrogen chemisorption as described in detail in [14].

4.1.3. Testing of catalyst coatings in microchannels

Six microstructured platelets were inserted inside the housing of the test reactor described in Section 3.1. Mass flow controllers regulated the gas flows. Water was dosed by a syringe pump, vaporized and then mixed into the gaseous reactants stream. The product gas analysis was carried out at the reactor exit by an Inficon Transpector CIS2 mass spectrometer.

The possible existence of temperature and concentration gradients was checked by calculating the proper criteria (Weisz modulus, Carberry number etc.). The details on these can be found in [14]. The conclusion of this analysis was that the flow inside the channels could be considered as plug flow, that no external mass and heat transfer resistances occurred and that the lowest catalyst efficiency factor was 0.95. Thus reaction rates measured in the microstructured testing device gave the intrinsic reaction rate.

Prior to the activity test, each batch of platelets was reduced in a flow of 10% hydrogen in argon (total flow of 200 Nml/min). The temperature was raised from 150 to 450 °C at a rate of 4 °C/min, and then kept at 450 °C for 30 min. Then reactor temperature was lowered to 200 °C in a flow of 10% H_2 in argon. The flow was then switched to pure argon and subsequently to the reactive flow. Two different feed compositions were tested: 10.0% CO, 20.0% H_2O, 30.0% H_2, 10.0% CO_2, 30.0% Ar corresponding to simulated reformate fed to HTS at four different total flow rates: 40–60–80–100 Nml/min and 2.6% CO, 27.5% H_2O, 33.8% H_2, 13.0% CO_2, 23.1% Ar for LTS at two different total flow rates: 100–200 Nml/min. This corresponds to a maximum WHSV of 9.5 Nl/(h g_{cat}) for HTS and 18.8 Nl/(h g_{cat}) for LTS. Fig. 6 shows the carbon monoxide conversion as a function of temperature at different total flows for HTS. From this Figure it is seen that above 280 °C the thermodynamic equilibrium composition at the reactor outlet is reached, indicating that no by-pass of the reaction mixture occurs. Fig. 7 shows the carbon monoxide conversion as a function of temperature at different total flows for LTS. The thermodynamic equilibrium composition at the reactor outlet is not completely reached, which was attributed to a certain by-pass flow which occurred owing to initial technical problems, namely tolerance of the platelet size, which had been solved for the HTS measurements discussed above.

4.1.4. Catalyst applied for the final 5 kW WGS reactors

The dimensions of the plates chosen to realize the 5 kW WGS units are reported in Table 1. Each plate contained 252 channels,

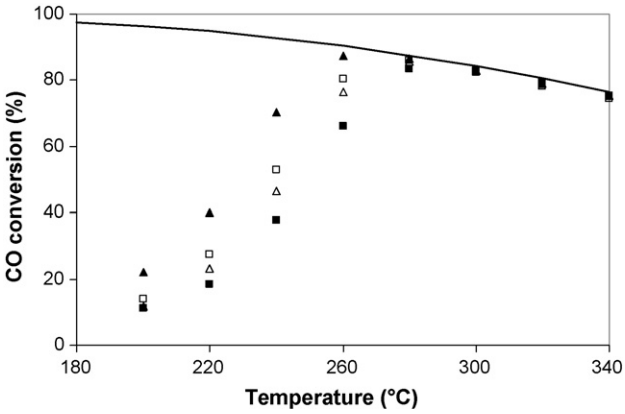

Fig. 6. Conversion of carbon monoxide over the microstructured $Pt/CeO_2/Al_2O_3$ catalyst as a function of the temperature. The full line is the calculated thermodynamic equilibrium of the WGS reaction. Reaction conditions: 10.0 vol.% CO, 20.0 vol.% H_2O, 30.0 vol.% H_2, 10.0 vol.% CO_2, 30.0 vol.% Ar. 6 platelets of 106 mg of catalyst each. (■) 100, (△) 80, (□) 60, (▲) 40 Nml/min.

126 on each side. These plates were heated for 10 h at 800 °C before the microchannels were filled with the alumina suspension. After drying at room temperature the alumina washcoat was calcined for 10 h at 600 °C. After this step the wash-coat was impregnated with a solution of $Ce(NO_3)_3 \times 6H_2O$ (31.7 g/l Ce), followed again by a calcinations step at 550 °C.

The platelets were impregnated by dipping them one by one for a few seconds into a vessel with a small amount of platinum solution (7.8 g/l platinum) and removing the excess of solution with compressed air. The removed excess of solution was recycled back into the impregnation basin. Fresh solution was poured into the vessel every few impregnations. The amount of deposited alumina was in average 2.1 ± 0.06 g per plate.

Some of the washcoat was scraped off and was used for characterization. Metal weight percentages measured by atomic emission spectroscopy are as follows: 0.9 wt.% platinum and 3.40 wt.% Ce. A specific surface area of the washcoat of 62 m^2/g was measured by N_2 adsorption. A platinum dispersion of 62%

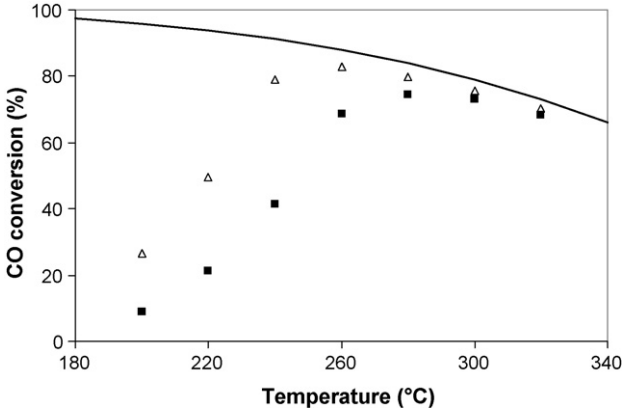

Fig. 7. Conversion of carbon monoxide over the microstructured $Pt/CeO_2/Al_2O_3$ catalyst as a function of the temperature. The full line is the calculated thermodynamic equilibrium of the WGS reaction. Reaction conditions: 2.6 vol.% CO, 27.5 vol.% H_2O, 33.8 vol.% H_2, 13.0 vol.% CO_2, 23.1 vol.% Ar. 4 platelets of 106 mg of catalyst each. (△) 100, (■) 200 Nml/min.

was measured by hydrogen chemisorption. Transmission electron microscopy was carried out on replicas of the catalyst sample. An average particle size of 2 nm was observed in good agreement with the hydrogen chemisorption data.

4.2. Preferential oxidation of carbon monoxide

Platinum-alumina catalysts were extensively studied and found very active towards carbon monoxide oxidation [15]; more recently platinum-supported zeolite catalysts were proposed thanks to their enhanced selectivity [16]. Previous studies on different Pt-3A zeolite catalysts [17] showed that the best catalytic performance, in terms of catalyst activity and selectivity, was obtained with a 1 wt.% Pt-3A zeolite catalyst, thanks to the specific structure of the 3A zeolite support.

4.2.1. Preparation

A catalyst consisting of 1% Pt over a mixed support 3A zeolite-Al_2O_3 was prepared via a slightly modified solution combustion synthesis (SCS) technique [18] at 500 °C, because of the presence of fine zeolite solid particles. As usual in SCS, $Al(NO)_3{\cdot}9H_2O$, urea and $Pt(NH_3)_4(NO_3)_2$ (as Al_2O_3 and Pt precursors: the nitrate form is compatible with the preparation method) were mixed together in an aqueous solution, then 3A zeolite fine particles – $K_{12}[(AlO_2)_{12}(SiO_4)_{12}]xH_2O$, from Fluka – were suspended in the solution, just to add the third catalyst component. After a few minutes stirring the suspension on a heating plate, to ensure proper homogeneity, the suspension was transferred in a bowl and placed into an oven kept at the constant temperature of 500 °C. First, the aqueous solution underwent dehydration, then, the mixture frothed and swelled, until a fast and highly exothermic reaction took place and, as is usual during SCS application, large amounts of gases evolved. The whole process extended over 5–6 min, but the time occurring between the actual ignition and the end of reaction was less than 10 s. A foamy and easily crumbled material was obtained to give a fine and volatile powder that was lastly finely ground in an agate mortar. Alumina precursors and zeolite were dosed in order to obtain a support composed by 50% b.w. zeolite and 50% b.w. alumina, and the prepared catalyst was indicated as 1% Pt-(50–50% mix).

The catalysts powder were pressed at 125 MPa into tablets, which were then crushed in an agate mortar and sieved to separate granules of 0.25–0.42 mm in size. The so-obtained catalyst particles were calcined in pure oxygen for 2 h at 350 °C to remove the nitrate ions and, in turn, to form a platinum oxide; the latter was then reduced in pure hydrogen for 2 h at 350 °C.

The subsequent step was the determination of the deposition procedure for the optimal catalyst deposition (a well stuck, adherent and compact catalyst layer) on the microchannel metal plate surface.

Then, a preliminary study was carried out on a lab microchannel reactor (platelets carrying channels 600 μm wide and 400 μm deep) with the aim to optimize the operative parameters affecting the structured catalyst performance in the view of its deposition inside the microchannels of the larger prototype reactor plates (5 kW).

Fig. 8. HRTEM of 1%Pt-(50–50% mix) powder catalyst, enlightened Pt clusters of 2–3 nm.

4.2.2. Catalyst characterisation

The obtained 1% Pt-(50–50% mix) catalyst in powder was analyzed by high-resolution transmission electron microscopy (HRTEM, Jeol JEM 2010 apparatus) to investigate the metal dispersion on the support. It was also examined by scanning electron microscopy and energy dispersion spectroscopy (SEM-EDS, LEO Supra 35) to evaluate the morphology and elemental distribution. Fig. 8 shows HRTEM picture enlighten the very good dispersion of Pt (cluster of 2–3 nm) over the mixed support 3A zeolite-Al_2O_3.

4.2.3. Fixed bed testing

The powdered catalyst was tested for the preferential CO oxidation with a synthetic reformate gas flow (0.5 vol.% CO, 1 vol.% O_2, 18 vol.% CO_2, 5 vol.% H_2O, 37 vol.% H_2 and He to balance, prepared by thermal mass-flow meters dosing of the component gases) in a temperature range of 100–300 °C. The CO and O_2 conversions and the oxygen selectivity to CO oxidation (assuming neither CO formation by reverse water–gas shift nor CO consumption by methanation) were determined. The employed reactor system and the bench rig scheme were described in detail in a previous work [17]. The experimental tests were carried out at O/CO feed ratio (λ) equal to 4 and with a weight hourly space velocity (WHSV) equal to 40 $Ndm^3/(h\ g_{cat})$.

The performance results, shown in Fig. 9, pointed out a complete CO conversion (for oxygen conversion equal to 1) in the temperature range ΔT_{CO} from 112 to 136 °C.

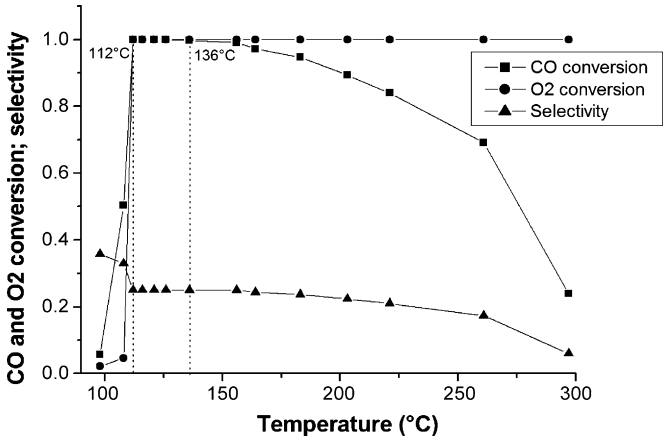

Fig. 9. CO conversion vs. temperature for 1 wt.% Pt-mix catalyst.

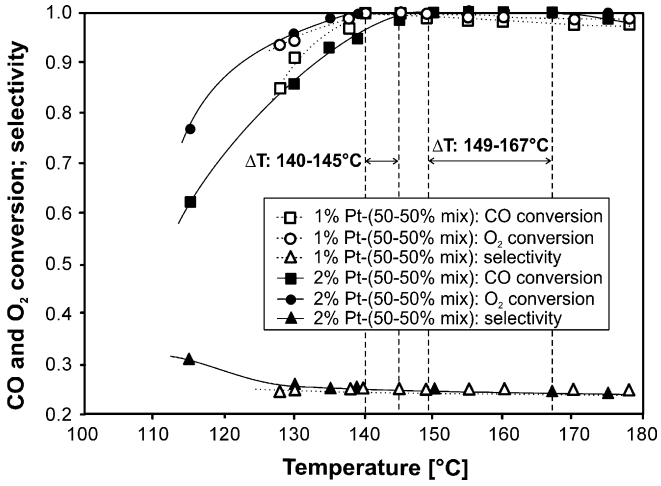

Fig. 11. CO conversion vs. temperature for 2 wt.% Pt-mix catalyst tested in the laboratory microchannel reactor.

4.2.4. Testing of catalyst coatings in microchannels

The second stage of the CO-PROX investigations was related to the behaviour analysis of the 1% Pt-(50–50% mix) as structured catalyst for microchannel reactors. Two different deposition methods were investigated for the microchannel coating: deposition of the precursors suspension into the plate channels by filling them with a syringe ("infusion pump" method) and "immersion" of metal plates stack in the precursors suspension. In both cases, after filling the channels, the catalyst layer was developed by SCS by placing the plates stack in the oven at 500 °C. SEM investigations (Fig. 10) on the microchannel catalyzed plates showed that the inner surface was covered more homogeneously and the channel ridge was cleaner when "infusion pump" method was used.

The "infusion pump" method was then chosen, since the desired catalyst layer formed quite exclusively inside the channels and the channel ridge was not involved; moreover, it guaranteed a lower consumption of the precursors suspension.

The operating conditions for catalytic activity tests on the lab microchannel reactor were as follows: WHSV = 25.5 $Ndm^3/(h\,g_{cat})$; synthetic feed mixture: 1 vol.% CO, 2 vol.% O_2, 18 vol.% CO_2, 5 vol.% H_2O, 37 vol.% H_2, He balance; $\lambda = 4$.

The test results, showed in Fig. 11, proved that the performance of the structured catalyst deposited into microchannel with a Pt loading of 1 wt.% was not satisfactory (residual CO < 10 ppm only in the temperature range ΔT_{CO} from 140 to 145 °C.); moreover, residual oxygen concentration was always present, also at high temperatures. Then, by doubling the Pt amount in the precursor suspension, a catalyst with 2% Pt was deposited by infusion method on microchannel plates. The complete CO conversion was then achieved, in the temperature range ΔT_{CO} of 149–167 °C (Fig. 11). A slight conversion shift towards higher temperatures could be observed, in comparison with the powdered catalyst tested in the fixed bed microreactor (ΔT_{CO} of 149–167 °C respect to 112–136 °C), probably due to the different system structure and, therefore, to the different heat transfer capability between the catalyst powder granules and the catalytic layer onto the microchannels.

4.2.5. Catalyst applied for the final 5 kW PrOx reactor

Thus the optimized catalyst, 2 wt.% platinum-mix (50% 3A zeolite + 50% alumina), was then deposed on the metal plates of larger sizes (120 mm × 200 mm × 1 mm; with 290 microchannels 600 μm wide and 400 μm deep, which were equally distributed on both sides of each plate).

The following deposition procedure was adopted:

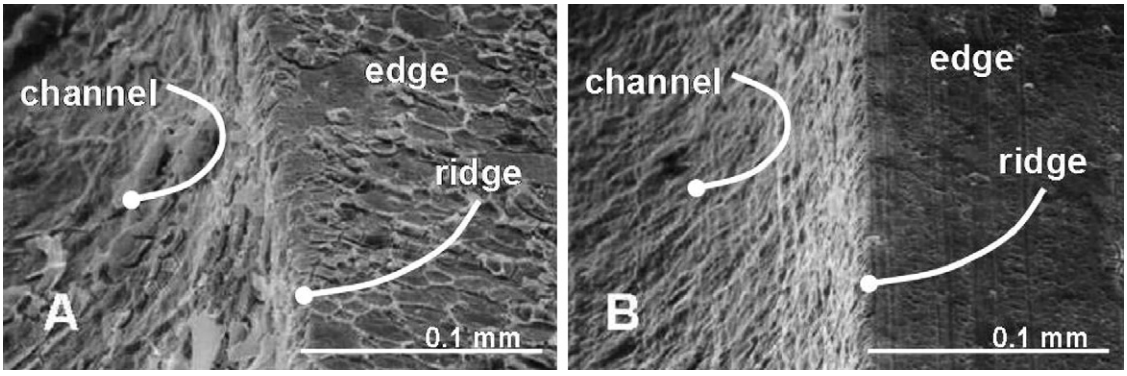

Fig. 10. SEM micrographs of 1% Pt-(50–50% mix) catalyst on microchannel plates deposited by "immersion" (A) and "infusion pump" (B) methods.

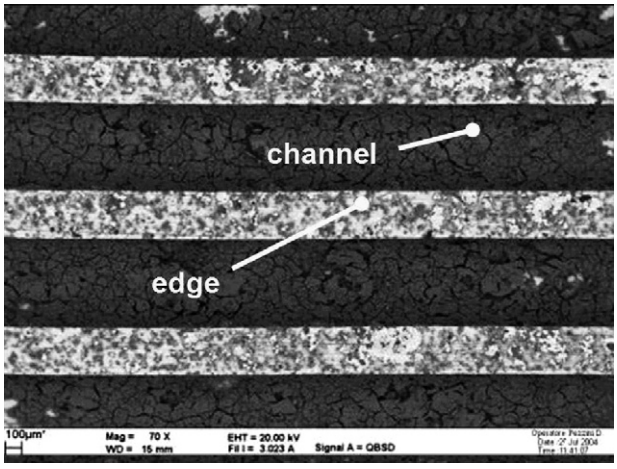

Fig. 12. SEM micrograph of catalysed microchannels on larger size metal plates.

- metal plates washing for 30 min with a solution of $K_2Cr_2O_7$, H_2SO_4 and distilled water, to eliminate possible organic contamination on the plates surface during machining;
- metal plates rinsing in distilled water;
- precursors solution/suspension deposition inside the microchannels of five plates stacked together with clamps by using the "infusion pump" method;
- elimination of the excess solution/suspension by spraying with compressed air at low flow rate;
- catalyst layer development by SCS of the stacked plates in an oven at 500 °C;
- spraying with compressed air to eliminate the excess not well stuck catalyst;
- repeated deposition procedures in order to reach the requested catalyst amount of 5 mg/cm^2 (1.15 g_{cat}/plate).

SEM micrographs (Fig. 12) showed a suitable and homogeneous catalyst distribution: the catalyst was mainly deposited inside the microchannels, whilst the ridges were satisfactory clean. This confirmed once again the effectiveness of the "infusion pump" method chosen before.

5. Testing of the final CO clean-up reactors

5.1. Experimental

In the previous paper [4] details of the set-up, which was used for testing of all final reactors are provided. Steam was generated externally by a conventional 8 kW evaporator and superheated to the appropriate reactor inlet temperature in a 3 kW microstructured gas heater and finally introduced into the reactor inlet. The carbon monoxide and carbon dioxide supply, which was performed separately as well as nitrogen for balancing the synthetic air feed and for purging the system was regulated by conventional thermal mass flow meters (Bronkhorst). The feed could be by-passed around the reactor. A pneumatically driven pressure control valve (Kemmer) regulated the system pressure.

Five (HTS) resp. six (LTS, PrOx) temperatures at the reactor body were monitored during the experiments. One temperature was measured at the reactor inlet (inside the diffuser upstream the perforated plate), three (HTS) resp. four (LTS, PrOx) temperatures in plate stack (see above). Finally the temperature of the product gases was determined in the outlet diffuser of the reactor.

The concentration of the various species present in the reactor off-gas was detected by an online micro gas chromatograph (Varian CP-4900 Micro-GC). It consisted of four different channels each with a separate TCD detector and oven. More details regarding the analytical procedure are provided in the previous paper [4]. A drawback of the fast analytical system was, that only a water content of less than 15 vol.% could be tolerated by the instrument. Thus all water was removed out of the gas flows before entering the GC by a tube filled with molecular sieve and results of analysis are reported on a dry basis (d.b.).

5.2. High temperature water–gas shift reactor

The composition and flow rates of the HTS reactor feed are shown in Table 2. They correspond approximately to the reformate produced by an autothermal reformer running at a steam to carbon (S/C) ratio of 3.3 and an oxygen to carbon (O/C) ratio around 0.68 at slightly higher nitrogen content to replace the methane usually present in reformate. Methane was not added to the feed because it was regarded as inert under the conditions of WGS. Basically, the steam, hydrogen, carbon dioxide and water flows were kept constant and the carbon monoxide flow was increased in three steps to evaluate the reactor performance under different load of carbon monoxide. The feed composition was determined when by-passing the reactor. It agreed well with the feed composition adjusted at a maximum deviation of 10% relative.

The electrical heating of the reactor was used for preheating to a temperature above 100 °C to avoid condensation.

Table 2
Feed composition—HTS reactor

	mmol/s	vol.%	(vol.%) d.b.
I. Total feed flow rate 152.7 Nl/min			
H_2O	41.9	36.9	n.d.
N_2	19.5	17.2	27.2
CO	4.1	3.6	5.7
CO_2	12.2	10.8	17.1
H_2	35.9	31.6	50.0
SUM	113.6	100.0	100.0
II. Total feed flow rate 155.0 Nl/min			
H_2O	41.9	36.4	n.d.
N_2	19.5	16.9	26.6
CO	5.8	5.0	7.9
CO_2	12.2	10.6	16.7
H_2	35.9	31.1	48.9
SUM	115.3	100.0	100.0
III. Total feed flow rate 158 Nl/min			
H_2O	41.9	35.6	n.d.
N_2	19.5	16.6	25.7
CO	8.2	7.0	10.8
CO_2	12.2	10.4	16.1
H_2	35.9	30.5	47.3
SUM	117.8	100.0	100.0

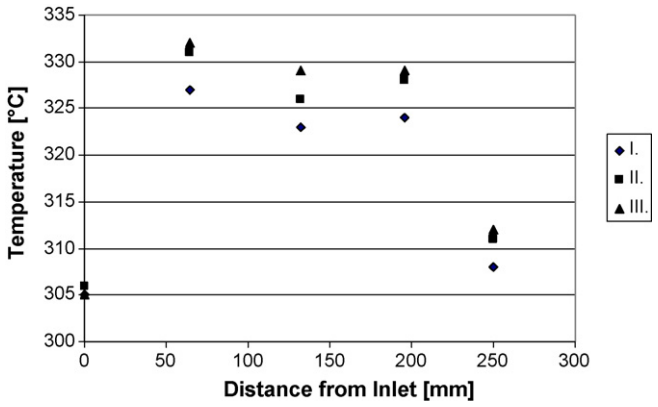

Fig. 13. Temperature profiles as determined for the HTS reactor; data sets refer to experimental conditions provided in Table 2.

Then a mixture of nitrogen and steam was used as heat carrier. The experiments were performed at a system pressure of 2.7 bar. The reactor was operated at low WHSV between 39 and 41 $Ndm^3/(h\ g_{cat})$.

The temperature profile of the reactor, which was determined during the experiments is provided in Fig. 13. The reactor temperature increased only moderately when increasing the carbon monoxide content of the feed and generally a flat temperature profile could be observed. The catalyst was not operated at temperatures exceeding 340 °C because loss of catalyst stability was expected.

Table 3 shows the product composition and carbon monoxide conversion as determined for different feed composition. For comparison the equilibrium conversion was calculated. The temperature determined at the last position downstream the plate stack ($x = 196$ mm) was chosen as temperature for these calculations. The conversion, initially at thermodynamic equilibrium for experiments I and II, decreased when the carbon monoxide concentration of the feed exceeded 5.0 vol% (wet basis) indicating the limitations of catalyst activity at reaction temperatures ranging between 320 and 335 °C.

The reactor was operated for a total duration of 4 h under different conditions. Attempts to improve its performance by increasing the feed temperature and simultaneous cooling of one or several zones with cooling air did not improve its performance even when the feed had the lowest content of carbon monoxide (3.6 vol.% wet base). The contrary was the case. Obviously the reactor temperature was at its lower limit already to achieve sufficient activity of the catalyst. On the other hand, the maximum operating temperature of 340 °C prohibited further improvement of the performance.

The heat generation by the water–gas shift reaction ranged between 145 (experiment I) and 265 W (experiment III). This heat was lost through the reactor insulation and the inlet- and outlet diffusers of the cooling channels to the environment.

Table 3
CO concentration of feed and product and conversion as determined for the HTS reactor

Dry base	CO (vol.%)	Conversion (%)	Eq. conversion (%)
I. Feed	5.7	–	–
I. Product	0.8	86.0	86.0
II. Feed	7.9	–	–
II. Product	1.0	88.0	87.6
III. Feed	10.8	–	–
III. Product	2.3	78.7	88.8

5.3. Low temperature water–gas shift reactor

The low temperature water–gas shift reactor (LTS) was fed with simulated HTS product. The composition and flow rates of the LTS reactor feed are shown in Table 4. Again, no methane was added. Different total flow rates and carbon monoxide concentration were investigated.

Pre-heating was performed in the same way as described for the HTS reactor above. The pressure ranged between 2.4 and 3.0 bar depending on the flow rate owing to limitations of the pressure control valve of the test rig. However, system pressure is not expected to affect the water–gas shift reaction significantly. The LTS reactor was operated at lower WHSV compared to the HTS reactor, which ranged between 17.7 and 32.1 $Ndm^3/(h\ g_{cat})$.

The temperature profile of the reactor, which was determined during the experiments, is shown in Fig. 14. Generally, it was slightly declining with a moderate temperature excursion at the plate stack outlet ($x = 196$ mm). This was attributed to the position of the thermocouples and their precision.

Table 5 shows the product composition and carbon monoxide conversion as determined for different feed concentration and reactor temperature. Again, equilibrium conversion was calculated for comparison. As described above for the HTS reactor, the temperature determined at the last position downstream the plate stack ($x = 196$ mm) was chosen as reaction temperature for the calculations. At the lower feed flow rate around

Table 4
Feed composition—LTS reactor

	mmol/s	vol.%	vol.% d.b.
I. Total feed flowrate 145.9 Ndm^3/min			
H_2O	40.6	37.4	0.0
N_2	17.9	16.4	26.3
CO	1.3	1.2	1.9
CO_2	13.7	12.6	20.1
H_2	35.2	32.4	51.8
SUM	108.6	100.0	100.0
II. Total feed flowrate 147.7 Ndm^3/min			
H_2O	40.6	36.9	0.0
N_2	17.9	16.2	25.8
CO	2.6	2.4	3.8
CO_2	13.7	12.5	19.7
H_2	35.2	32.0	50.8
SUM	109.9	100.0	100.0
III. Total feed flowrate 197.0 Ndm^3/min			
H_2O	55.6	37.9	0.0
N_2	26.0	17.8	28.6
CO	1.8	1.2	2.0
CO_2	12.6	8.6	13.8
H_2	50.6	34.5	55.6
SUM	146.6	100.0	100.0

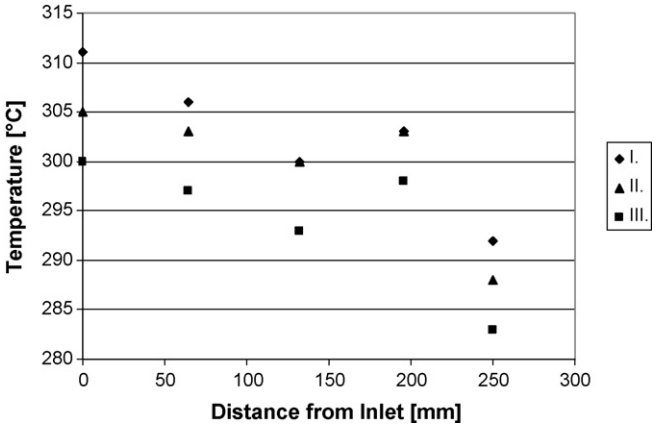

Fig. 14. Temperature profile as determined for the LTS reactor; data sets refer to experimental conditions provided in Table 4.

80 Ndm^3/min, conversion, initially at thermodynamic equilibrium (experiment I), increased with increasing content of carbon monoxide in the feed (experiment II) but thermodynamic equilibrium could not be achieved any more. Similar to the HTS this was regarded as a limitation of catalyst activity, because at higher feed flow rate but 5 K lower reaction temperature equilibrium conversion was achieved again (experiment III, Table 5). Between 40 and 80 W of heat were generated by the reaction, which was lost to the environment.

5.4. Reactors for the preferential oxidation of carbon monoxide

5.4.1. First stage carbon monoxide PrOx reactor

Simulated LTS product was fed to the 1st stage preferential oxidation reactor (PrOx1). Composition and flow rates of the PrOx1 reactor feed are shown in Table 6. The reactor was tested at different temperatures, feed flow rates and λ(O/C ratio). Different to the WGS reactors the PrOx reactors were not pre-heated electrically but exclusively by pre-heated nitrogen. The experiments were performed at a system pressure between 1.9 and 3.3 bar depending on the feed flow-rate. The reactor was operated at WHSV between 48.0 and 98.0 $Ndm^3/(h\ g_{cat})$.

Fig. 15 shows the hydrogen and carbon monoxide conversion as determined for the reactor versus the reactor temperature at λ(O/CO) 3.9 and a pressure of 1.9 bar. For the sake of simplicity, an average reactor temperature was calculated. The reactor temperature was set by adjusting the cooling gas flow. Under

Table 5
CO concentration of feed and product and conversion as determined for the LTS reactor

	Temperature (°C)	Dry base CO (vol.%)	Conversion (%)	Eq. conversion (%)
I. Feed	–	1.9	–	–
I. Product	303	0.55	71.1	71.6
II.Feed	–	3.8	–	–
II. Product	303	0.90	76.3	85.0
III. Feed	–	2.0	–	–
III. Product	298	0.40	80.0	81.0

Table 6
Feed composition—PrOx1reactor

I. Total flow rate		102.5	Ndm^3/min
	λ(O/CO)	2.2	
	mmol/s	vol.%	(vol.%) d.b.
H_2O	35.0	45.9	0.0
N_2	11.4	15.0	27.6
O_2	0.3	0.4	0.7
CO	0.3	0.3	0.6
CO_2	8.5	11.1	20.6
H_2	20.8	27.3	50.5
SUM	76.3	100.0	100.0
II. Total flow rate		103.9	Ndm^3/min
	λ(O/CO)	3.9	
	mmol/s	vol.%	(vol.%) d.b.
H_2O	35.0	45.3	0.0
N_2	12.2	15.8	28.9
O_2	0.51	0.7	1.2
CO	0.26	0.3	0.6
CO_2	8.5	11.0	20.0
H_2	20.8	26.9	49.2
SUM	77.3	100.0	100.0
III. Total flow rate		105.5	Ndm^3/min
	λ(O/CO)	5.7	
	mmol/s	vol.%	(vol.%) d.b.
H_2O	35.0	44.6	0.0
N_2	13.2	16.8	30.3
O_2	0.7	1.0	1.7
CO	0.3	0.3	0.6
CO_2	8.5	10.8	19.5
H_2	20.8	26.5	47.9
SUM	78.5	100.0	100.0
IV. Total flow rate		106.8	Ndm^3/min
	λ(O/CO)	7.3	
	mmol/s	vol.%	(vol.%) d.b.
H_2O	35.0	44.0	0.0
N_2	13.9	17.5	31.3
O_2	1.0	1.2	2.1
CO	0.3	0.3	0.6
CO_2	8.5	10.7	19.1
H_2	20.8	26.2	46.9
SUM	79.5	100.0	100.0
V. Total flow rate		184.7	Ndm^3/min
	λ(O/CO)	4.1	
	mmol/s	vol.%	(vol.%) d.b.
H_2O	55.6	40.4	0.0
N_2	24.7	18.0	30.2
O_2	1.0	0.8	1.3
CO	0.5	0.4	0.6
CO_2	13.6	9.9	16.6
H_2	42.0	30.6	51.3
SUM	137.5	100.0	100.0

Table 6 (*Continued*)

VI. Total flow rate		208.2	Ndm^3/min
	λ(O/CO)	4.0	
	mmol/s	vol.%	(vol.%) d.b.
H_2O	55.6	35.9	0.0
N_2	33.5	21.6	33.7
O_2	1.3	0.8	1.3
CO	0.6	0.4	0.6
CO_2	11.4	7.3	11.5
H_2	52.6	34.0	52.9
SUM	154.9	100.0	100.0

Table 7
CO and H_2 conversion and concentration of unconverted O_2 vs. λ(O/CO) as determined for the PrOx1 reactor

Total flow rate (Ndm^3/min)	λ(O/CO) (−)	Reaction temperature (°C)	Conversion	
			CO (%)	H_2 (%)
I. 102.5	2.2	179	38.7	3.1
II. 103.9	3.9	182	60.5	3.9
III. 105.5	5.8	183	90.2	5.3
IV. 106.8	7.3	177	88.5	5.5
V. 184.7	4.1	206	90.8	7.8

these conditions, energy generation amounted up to 300 W in the reactor, which was partially removed by cooling the first and second stage with 30 Ndm^3/min air each, corresponding to a heat removal of 225 W. The remaining heat was lost to the environment. Conversion of carbon monoxide increased significantly from 50% to more than 90% with increasing reactor temperature, while hydrogen conversion remained at low values between 3 and 5%.

The next set of experiments was performed at different values of λ(O/CO) at reactor temperatures around 180 °C. Again, the cooling gas flow was used to achieve approximately the same temperature despite the significant heat generation especially at high values of λ(O/CO). When increasing λ(O/CO) from 2.2 to 5.8, carbon monoxide conversion increased significantly from 38.7 to 90.2% (see Table 7). This went along with increasing hydrogen conversion. Further increase of λ(O/CO) to 7.3 did not improve the reactor performance. However, hydrogen conversion increased further. This indicated that the catalyst had reached its optimum performance under these conditions. When further increasing the feed flow rate to 185 Ndm^3/min and reactor temperature to 206 °C in parallel (last line of Table 7), a similar degree of conversion could be achieved, however, along with higher hydrogen conversion.

Table 8
Feed composition—PrOx2reactor

Total flow rate		209.9 (Ndm^3/min)	
	λ(O/CO)	3.9	
	mmol/s	vol.%	(vol.%) d.b.
H_2O	55.6	35.6	0.0
N_2	26.5	17.0	26.4
O_2	0.13	0.08	0.13
CO	0.07	0.04	0.07
CO_2	21.1	13.5	20.9
H_2	52.8	33.8	52.5
SUM	156.2	100.0	100.0

Hence the catalyst could be operated at four times higher space velocities compared to the initial experiments performed in the small scale reactor, when the reaction temperature was increased to values between 180 and 210 °C. However, the conversion was incomplete under these conditions as already indicated in Fig. 15.

5.4.2. Second stage CO PrOx reactor

The 2nd stage preferential oxidation reactor (PrOx2) was fed with simulated product of PrOx1. The composition and flow rates of the PrOx2 reactor feed are shown in Table 8. The reactor was tested at different temperatures. Again the reactor was pre-heated with nitrogen. The experiments were performed at a system pressure of 3.3 bar. The reactor was operated at WHSV of 98.0 $Ndm^3/(h\ g_{cat})$.

Fig. 16 shows the carbon monoxide conversion as determined for the reactor versus the reactor temperature at λ(O/CO) 3.9. Again, an average reactor temperature was calculated. The reactor temperature was set by adjusting the feed temperature. Under these conditions, energy generation amounted up to 50 W in

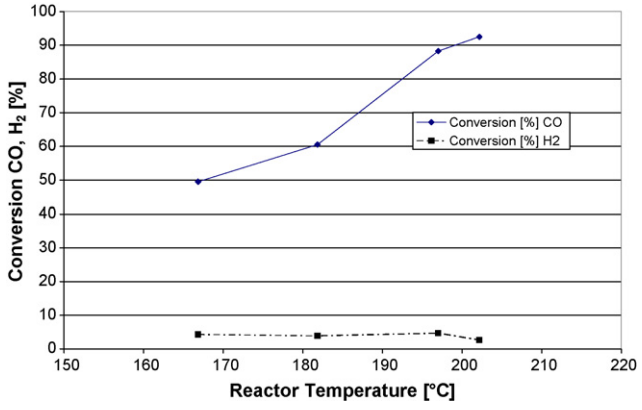

Fig. 15. CO and H_2 conversion and concentration of unconverted O_2 vs. reactor temperature as determined for the PrOx1 reactor at λ(O/CO) = 3.9.

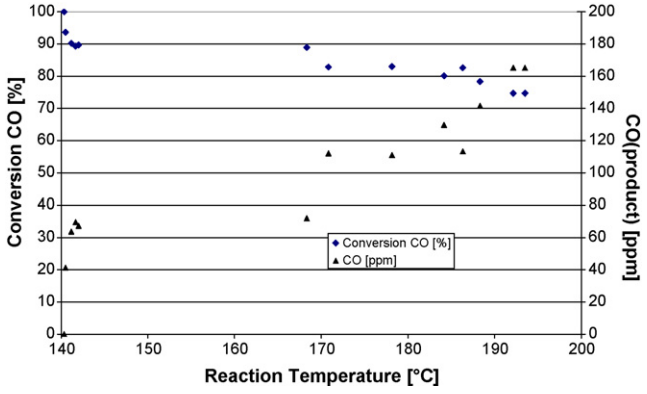

Fig. 16. CO vs. reactor temperature as determined for the PrOx2 reactor at λ(O/CO) = 3.9.

the reactor, which was lost to the environment. Different to the PrOx1 reactor, conversion of carbon monoxide increased significantly from 75% to more than 90% with decreasing reactor temperature which is attributed to the reverse water–gas shift reaction getting dominant at higher reaction temperature and low concentration of carbon monoxide. Ninety percent conversion corresponds to a carbon monoxide concentration of approximately 50 ppm, which is regarded as sufficient for a carbon monoxide tolerant low temperature PEM fuel cell operated with air bleed to the anode.

The HTS, LTS and PrOx1 reactors were removed from the test rig after testing and subsequently incorporated into a complete fuel processor. Results from the operation of this fuel processor will be reported below.

6. Assembly and testing of the fuel processor

6.1. Experimental set-up

Fig. 17 shows the flow scheme of the fuel processor, which was arranged on a bread-board level at IMM.

Water and iso-octane were provided by metering pumps through thermal mass flow meters (FIRC 101 and 102) to Evaporator 1 and 2 respectively. The exit temperatures of vapours were regulated by temperature controllers of the evaporators. Nitrogen (FIRC 111) and oxygen (FIRC 112) were dosed separately into the gas mixer (T-junction), where they were mixed with the steam from Evaporator 1. After pre-heating the air/steam mixture in heated tubing with separate temperature control it entered an electrically heated gas-heater, which pre-heated the feed (not the iso-octane) to a temperature of 720 °C. The feed then entered the inlet diffuser of the autothermal reformer (ATR), where it was blended with the iso-octane from evaporator 2. The ATR reactor, its features and performance in separate testing is described in a previous paper [4]. Downstream the ATR, a micro-structured heat-exchanger (not shown here) was incorporated between the ATR and the HTS reactor to cool down the reformate from the exit temperature of the ATR to the desired feed temperature of the HTS. It had a heat-exchange capacity of up to 2 kW under operating conditions. Pressurised air was applied as cooling agent.

The reformate then entered the HTS, LTS and PrOx1 reactors subsequently. It could be by-passed around all further reactors down-stream (HTS, LTS and PrOx1) directly to the common exhaust system, which was still upstream the pressure control valve (PIRC 601) and the exhaust cooler/condenser. Additionally, sample lines allowed for GC analysis up-and downstream the ATR, and downstream the HTS, LTS and PrOx1. Again online (Micro-)GC analysis was applied for chemical analysis of the reformate. Thus an overview of the performance of all reactors of the fuel processor could be gained within less than 15 min. Downstream the LTS, a water injection (WI 3) was installed to

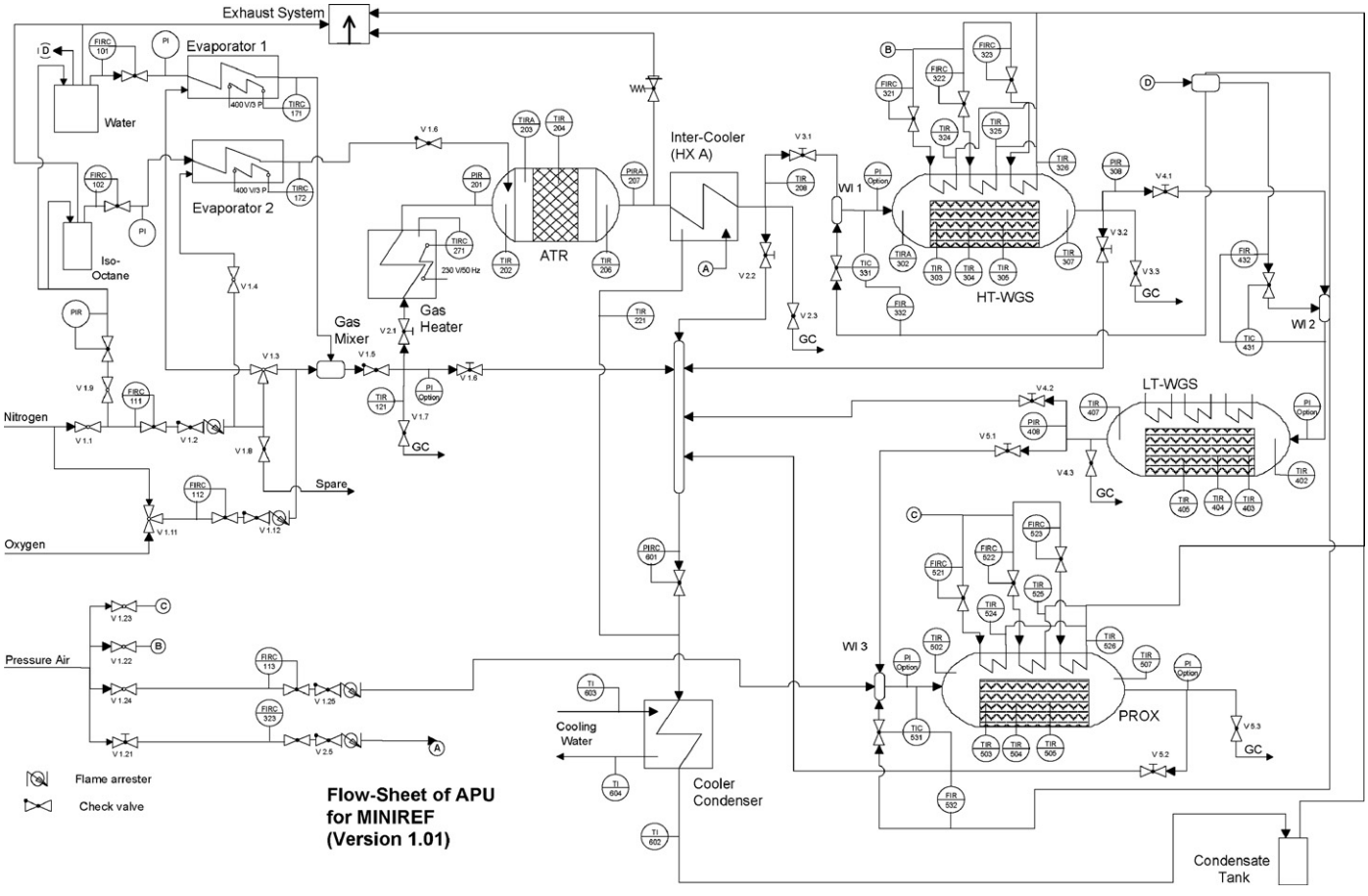

Fig. 17. Flow scheme of the fuel processor.

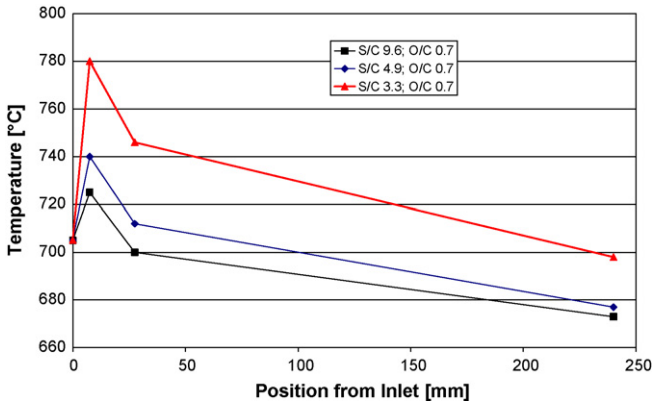

Fig. 18. Temperature profile of the ATR reactor vs. S/C ratio as determined during the fuel processor tests.

further cool the reformate to the inlet temperature of PrOx1. At the same position air was fed to the reformate. A total of 33 temperatures, 5 pressures and 13 flows were registered by a data acquisition system.

6.2. Results and discussion

To achieve the desired power output of 5 kW_{el} the following molar flow rates had to be fed to the fuel processor according to the system design: 73 mmol/s water, 34 mmol/s air and 2.7 mmol/s iso-octane. This corresponds to S/C ratio of 3.3 and O/C ratio of 0.67. However, limitations of the feeding system, namely evaporator 1, limited the experiments to 73% of the design capacity. The tests were performed by setting nitrogen and steam flows to the final value, while iso-octane and oxygen were increased in parallel maintaining constant O/C ratio. Thus the S/C ratio was decreased step by step. Table 9 shows the feed compositions which correspond to 25% (test I), 50% (test II) and 73% (test III) of the design capacity. After stable operation was achieved in the ATR under the conditions of test I, the reformate, which was by-passed around the clean-up reactors before, was passed through them for the further tests. The air flow fed to the PrOx reactor was increased in parallel from test I to test III. Practically, the λ(O/CO) ratio was decreasing from test I (λ = 5.0) to test III to λ = 2.5.

The ATR reactor converted—similar to the single tests described in a previous paper [4] more than 98% of the iso-octane. With decreasing S/C ratio, the hot spot temperature increased until it reached a maximum of 80 K (see Fig. 18). Fig. 19 shows the product composition of the ATR versus the S/C ratio. As expected according to the thermodynamic equilibrium, both carbon monoxide (WGS), methane (methanation) and light alkene formation decreases at higher S/C ratio. Table 10 shows a heat balance of the reactor. Not only the partial oxidation reaction, but also the water–gas shift and methanation reactions contributed significantly to the heat generation in the reactor. Approximately 300 W of energy were lost through the insulation, which would require improvement in a later system.

Table 11 shows the pressures determined over the reactors. While a pressure drop of approximately 100 mbar was determined for the ATR reactor, the pressure drop of the clean-up

Table 9
Feed composition—fuel processor

Total flow rate		102.6	Ndm^3/min
S/C	10.0	O/C	0.68
	(mmol/s)	(vol.%)	(vol.%) d.b.
I. ATR			
H_2O	54.8	71.8	0.0
N_2	19.0	24.9	88.2
O_2	1.9	2.4	8.6
C_8H_{18}	0.7	0.9	3.2
SUM	76.3	100.0	100.0
	λ(O/CO) (mmol/s)	5.00	
I. PrOx			
Air	0.6	–	–
H_2O	6.2	–	–
Total flow rate		106.0	Ndm^3/min
S/C	5.0	O/C	0.68
	(mmol/s)	(vol.%)	(vol.%) d.b.
II. ATR			
H_2O	54.8	69.4	0.0
N_2	19.0	24.0	78.7
O_2	3.8	4.8	15.6
C_8H_{18}	1.4	1.8	5.7
SUM	78.9	100.0	100.0
	λ (O/CO) (mmol/s)	3.70	
II. PrOx			
Air	1.1	–	–
H_2O	6.2	–	–
Total flow rate		109.4	Ndm^3/min
S/C	3.3	O/C	0.68
	(mmol/s)	(vol.%)	(vol.%) d.b.
III. ATR			
H_2O	54.8	67.3	0.0
N_2	19.0	23.3	71.2
O_2	5.6	6.9	21.0
C_8H_{18}	2.1	2.5	7.7
SUM	81.4	100.0	100.0
	λ(O/CO) (mmol/s)	2.10	
III. PrOx			
Air	1.7	–	–
H_2O	6.2	–	–

Table 10
Heat balance of the ATR reactor at 73% of the design capacity

	Heat input/generation	Heat output/consumption
Temperature (°C)	705	698
Forced convection (W)	1857	2200
Partial oxidation (W)	852	
Water–gas shift (W)	308	
Methanation (W)	413	
Steam reforming (W)		929
Losses (W)		302
Total (W)	3430	3430

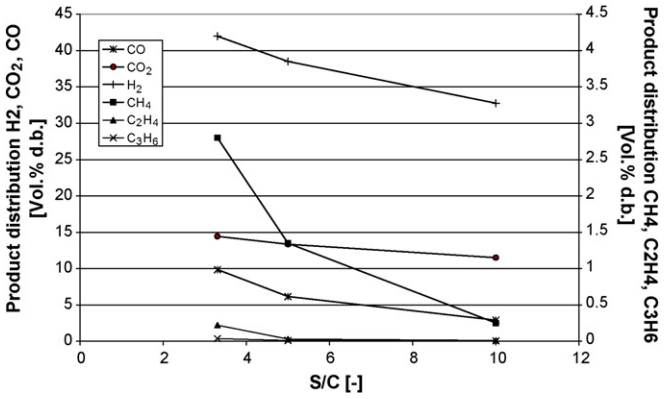

Fig. 19. Reformate composition (vol.% d.b.) as determined downstream the ATR reactor vs. S/C ratio.

reactors was in the range of 200 mbar. This higher pressure drop originated from the tubing and valves rather than from the reactors. Table 11 also shows the settings and performance of the cooling equipment of the fuel processor. The compact heat exchanger (HX; plate stack volume about 50 cm^3) downstream the ATR transferred up to 916 W of energy to 80 Ndm^3/min cooling air. The reformate was cooled from 698 to 323 °C under these conditions. The HTS reactor was operated without cooling gas. Upstream the PrOx1 reactor, the reformate was cooled to 200 °C by the water injection (WI). In the PrOx1 reactor, only the first cooling stage was used, which removed up to 160 W heat generated by the hydrogen and carbon monoxide oxidation reactions.

The performance of the clean-up reactors is summarised in Table 12. While the HTS showed high (equilibrium) conversion at 25% and 50% of the design capacity, conversion decreased significantly at 73% of the design capacity. This could not be prevented by increasing the average reactor temperature from 320 to 330 °C. Similar to the single HTS tests, conversion at 73% of the design capacity was at 88% slightly below equilibrium conversion (93%). However, the LTS, working between 300 and 310 °C, showed very low conversion at 25% and 50% of the design capacity, because the equilibrium was already set

Table 11
System pressures and performance data of the cooling equipment of the fuel processor

	I S/C = 10.0	II S/C = 5.0	III S/C = 3.3
p_{in}ATR (bar)	3.0	3.8	4.1
p_{out} ATR (bar)	2.9	3.7	4.0
p_{out}HTS (bar)	2.4	3.2	3.5
p_{out}LTS (bar)	2.3	3.0	3.3
p_{out}PrOx (bar)	2.0	2.8	3.1
$T_{in,reformate}$HX (°C)	673	677	698
$T_{out,reformate}$HX (°C)	430	322	323
$T_{out,cooling\ air}$HX (°C)	407	459	484
Cooling gas HX (Ndm^3/min)	30	70	80
Cooling power HX (W)	283	755	916
Heat transf. eff. HX (%)	32	54	58
Heat transf. coeff. HX (W/(m^2K))	18	64	78
Water flow WI (g/min)	6.7	6.7	6.7
Cooling power WI (W)	313	313	313
$T_{out,cooling\ air}$PrOx1 (°C)	–	160	200
Cooling gas PrOx1 (Ndm^3/min)	0	12	42
Cooling power PrOx1 (W)	0	38	170

Table 12
Performance of the CO clean-up reactors

	I. S/C = 10.0	II. S/C = 5.0	III. S/C = 3.3
Temperature HT-WGS (°C)	322	316	329
Conversion HT-WGS (%)	94	93	88
Temperature LT-WGS (°C)	301	304	310
Conversion LT-WGS (%)	10	16	40
Temperature PrOx1 (°C)	185	196	208
Conversion PrOx1 (%)	100	92	96
Conc. CO PrOx1 exit (ppm)	0	225	200
Fuel processor efficiency (%)	88	79	74

by the HTS. At 73% of the design capacity the LTS took over a significant part of the CO conversion, namely 40%. Severin et al. found different degrees of conversion for their monolithic WGS reactors operated in a 3 kW gasoline fuel processor [19]. Because they operated conventional HTS and LTS catalysts around 450 °C and 300 °C respectively, the conversion in their HTS reactor was limited by the equilibrium and amounted to only 65%, whereas the LTS showed high conversion around 80%.

The PrOx1 reactor converted the CO completely (below detection limit of 5 ppm) at 25% of the design capacity. At higher flow rates, more than 90% conversion could be achieved. At 73% of the design capacity, the reformate contained 200 ppm of carbon monoxide, which was comparable to the results achieved for the single reactor, however, at a much lower λ(O/CO). The heat generated by the oxidation reactions amounted to 240 W.

Fig. 20 shows the result of GC analysis determined after each reactor at 73% of the fuel processor design capacity (test III). Within each set of piles referring to the different gases present in the reformate, the different colours refer to the reactors subsequently from left to right. The different values determined for each species and each reactor refer to samples taken with the course of time within 150 min of operation of the fuel processor under these conditions. The analysis shows stable performance of the fuel processor. The content of nitrogen remains constant from ATR to HTS as expected and increases slightly downstream the PrOx1 owing to the air addition to the PrOx1 feed. Methane remained constant as well, however, after PrOx1 the

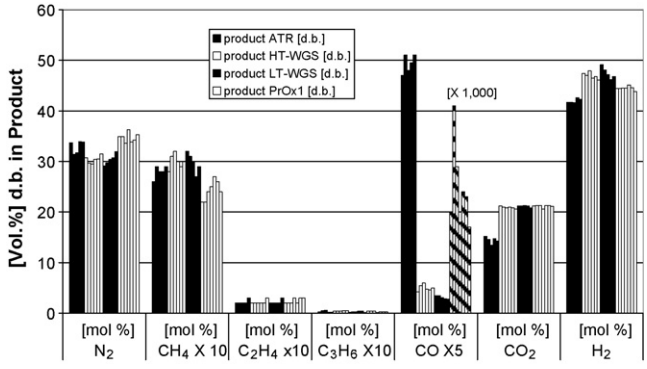

Fig. 20. Reformate composition (vol.% d.b.) as determined downstream the fuel processor reactors at 73% of design capacity; for each species from left to right: ATR product samples; HTS product samples; LTS product samples; PrOx1 product samples; values of CH_4, C_2H_4 and C_3H_6 are magnified by a factor of 10; values of CO are magnified by a factor of 5; CO content of PrOx1 product (ppm; hatched piles) by a factor of 1000.

values of methane were significantly lower. The dilution by air addition was not sufficient to explain the decreasing methane content and thus the conclusion could be drawn, that methane was irreversibly adsorbed in PrOx1, which would lead to catalyst deactivation by coke formation. Within the scope of the measurements, no deactivation of the catalyst was observed. Ethylene concentration was very low (0.2–0.3 vol.%) and remained constant within the accuracy of the analysis. Propylene, present with one order of magnitude lower concentration (0.06–0.03 vol.%) could also be detected after the PrOx1 reactor. Carbon monoxide concentration decreases according to the clean-up procedure and carbon dioxide increases. However, the increase of carbon dioxide downstream LTS and PrOx1 is within the range of accuracy of the measurements. Finally the hydrogen content increases by WGS and decreases again owing to the hydrogen consumption in PrOx1. The dry hydrogen content amounted to approximately 44 vol.%, which corresponds to 24 vol.% on a wet basis. 46 vol.% of steam were contained in the reformate after PrOx1, which is slightly below the dewpoint at 80 °C (operating temperature of the fuel cell). The overall fuel processor efficiency was calculated according to the following formula:

$$\eta = \frac{\dot{n}_{H_2} \mathrm{LHV}_{H_2}}{\dot{n}_{C_8H_{18}} \mathrm{LHV}_{C_8H_{18}}}$$

revealing 74% efficiency at 73% of the design capacity. This value is lower compared to the results from testing of the single ATR reactor, which were closer to 80%. This is attributed to the increasing methane formation in the ATR which in turn is indicating an aging of the ATR catalyst during the experiments. In the last line of Table 12, the efficiency calculated for different S/C ratio is shown. Owing to the lower methane and light alkene formation, the efficiency increases with increasing S/C ratio. The conclusion is nevertheless misleading, that more water addition is beneficial for the system efficiency. Water requires energy for preheating, evaporation and superheating, which could be partially provided by condensing water out of the reformate after the PrOx reactor. However, in practical systems energy losses require consideration. Thus an increased water addition to the feed would require lower utilisation of the hydrogen in the fuel cell anode to provide sufficient energy to an afterburner, which in turn supplies heat to the evaporator of the fuel processor. Thus the overall fuel processor efficiency should be calculated taking into consideration both fuel and anode off-gas hydrogen consumption. However, anode off-gas recirculation would have exceeded the scope of the work presented here.

6.3. Outlook

The autothermal reforming of fuels is a viable option for hydrogen supply to fuel cells. However, steam reforming has significant advantages, namely higher system efficiency [20]. Thus work is on its way at IMM in the scope of different projects to realise steam reformers for LPG and diesel in integrated microstructured heat-exchanger/reactors for fuel cell applications in the power range of 250 W and 5 kW, respectively. Co- and counter-current arrangements of flows are applied in these reactors in order to further improve efficiency compared to the cross-flow design presented here.

Acknowledgement

The authors gratefully acknowledge the financial support of this work by the European Commission in the scope of the project MINIREF contract-no.: ENK6-CT-2001-00515.

References

[1] G. Kolb, V. Hessel, Review: micro-structured reactors for gas phase reactions, Chem. Eng. J. 98 (2004) 1.
[2] V. Hessel, H. Löwe, A. Müller, G. Kolb, Chemical Micro Process Engineering—Vol. 2: Processing Applications and Plants; Chapter 2: Microstructured Fuel Processors for Energy generation, Wiley, Weinheim, 2005, ISBN 13-978-3-527-30998-6, 281 ff.
[3] R.E. Delsman, M.H.J.M. de Croon, A. Pierik, G.J. Kramer, P.D. Cobden, Ch. Hofmann, V. Cominos, J.C. Schouten, Chem. Eng. Sci. 59 (2004) 4795–4802.
[4] G. Kolb, T. Baier, J. Schürer, D. Tiemann, A. Ziogas, H. Ehwald, P. Alphonse, A micro-structured 5 kW complete fuel processor for iso-octane as hydrogen supply system for mobile auxiliary power units; Part I—development of autothermal reforming catalyst and reactor, Chem. Eng. J. 137 (2008) 653–663.
[5] J.M. Moe, Chem. Eng. Pro. 58 (1962) 33.
[6] M.V. Twigg (Ed.), Catalyst handbook, 2nd Ed., Wolfe Press, London, 1989, Chapter 6: water–gas shift.
[7] M.V. Twigg, M.S. Spencer, Appl. Catal. A: Gen. 212 (2001) 161.
[8] V. Cominos, V. Hessel, C. Hofmann, G. Kolb, R. Zapf, A. Ziogas, E.R. Delsman, J.C. Schouten, Catal. Today 110 (2005) 140.
[9] V. Cominos, S. Hardt, V. Hessel, G. Kolb, H. Löwe, M. Wichert, R. Zapf, Chem. Eng. Commun. 192 (2005) 685–698.
[10] R.K. Ahluwalia, Q. Zhang, D.J. Chmielewski, K.C. Lauzze, M.A. Inbody, Catal. Today 99 (2005) 271–283.
[11] L. Mendelovici, M. Steinberg, J. Catal. 96 (1985) 285.
[12] S. Hilaire, X. Wang, T. Luo, R.J. Gorte, J. Wagner, Appl. Catal. A: Gen. 215 (2001) 271.
[13] G. Kolb, H. Pennemann, R. Zapf, Catal. Today 110 (2005) 121.
[14] G. Germani, Y. Schuurman, AIChE J. 52 (2006) 1806–1813.
[15] M.J. Kahlich, H.A. Gasteiger, R.J. Behm, J. Catal. 171 (1997) 93.
[16] H. Igarashi, H. Uchida, M. Suzuki, Y. Sasaki, M. Watanabe, Appl. Catal. A 159 (1997) 159.
[17] I. Rosso, C. Galletti, G. Saracco, E. Garrone, V. Specchia, Appl. Catal. B 48 (2004) 195–203.
[18] K.C. Patil, S.T. Aruna, T. Mimani, Solid State Mater. Sci. 6 (2002) 507.
[19] C. Severin, S. Pischinger, J. Ogrzewalla, J. Power Sources 145 (2005) 675–682.
[20] A. Cutillo, S. Specchia, M. Antonini, G. Saracco, V. Specchia, J. Power Sources 154 (2006) 379–385.